Advanced Physical Research
Vol.8, No.1, 2026, pp.52-64
https://doi.org/10.62476/apr.8152

A FIRST-PRINCIPLES STUDY OF STRUCTURAL REORGANIZATION AND METALLIZATION IN Fe-SUBSTITUTED $CrPSe_3$

Nguyen Phuc[1], **T.A. Tran**[1], **H.C. Tran**[1], **A.M. Yariyeva**[2], **M.E. Aliyev**[3], **L.V. Truong-Son**[4,1*]

[1]Department of Engineering Physics, Ho Chi Minh City University of Technology and Engineering, Ho Chi Minh, Vietnam
[2]Azerbaijan Technical University, Baku, Azerbaijan
[3]Nakhchivan State University, Nakhchivan, Azerbaijan
[4]The University of Danang - University of Science and Education, Danang, Vietnam

Abstract. Chemical substitution offers a powerful route for engineering electronic phases in two-dimensional (2D) van der Waals materials, particularly in systems where structural distortions and ligand-field asymmetry strongly influence electronic behavior. In this work, we perform a comprehensive first-principles investigation of pristine and Fe-substituted monolayer $CrPSe_3$ to elucidate the structural and electronic mechanisms that drive its semiconductor-to-metal transition. The optimized pristine structure reproduces experimentally reported bond lengths and angular distortions, confirming the reliability of our computational baseline. Fe incorporation induces pronounced anisotropic lattice relaxation, including a substantial reduction in the monoclinic angular disparity of the honeycomb network and significant reorganization of metal-chalcogen bonding. Charge-state analysis shows that Fe donates considerably fewer electrons to Se than Cr, enhancing Fe–Se covalency and shifting Fe *3d* states into the narrow band gap of pristine $CrPSe_3$. These structural and chemical perturbations collectively increase *p-d* hybridization, broaden frontier bands, and generate a metallic electronic structure characterized by hybrid Fe/Cr t_{2g} states crossing the Fermi level. The results establish a coherent mechanistic framework linking lattice symmetry, bonding character, and orbital hierarchy, and demonstrate that the transition-metal substitution provides an effective pathway for tuning electronic phases in MPX_3 monolayers.

Keywords: $CrPSe_3$, MPX_3, Fe-doping, density functional theory, 2D materials, electronic structure.
Corresponding author: Le Vu Truong-Son, The University of Danang - University of Science and Education, 550000 Danang, Vietnam, e-mail: *lvtson_kl@ued.udn.vn*
Received: 4 September 2025; Revised: 22 November 2025; Accepted: 12 January 2026; Published: 18 February 2026.

1 Introduction

Studying the structure and physical properties of functional materials expands their application potential. Therefore, extensive research is being conducted on the structure, optical, and magnetic properties of materials with various properties. Chalcogenide semiconductors occupy a special place among these materials. In addition to their highly symmetrical crystalline structure, these materials also exhibit layered and chain structures (Kitano et al., 2013; Asgerov et al., 2018; Tran et al., 2024).

Two-dimensional (2D) van der Waals (vdW) materials have rapidly evolved into a versatile platform for uncovering emergent quantum phenomena and for engineering tunable electronic, optical, and magnetic functionalities. Since the advent of graphene, an increasingly broad class

of layered compounds - including transition-metal dichalcogenides, group-III chalcogenides, and 2D magnetic semiconductors - has revealed an exceptional degree of structural and electronic adaptability under reduced dimensionality. This adaptability enables precise manipulation of band topology, carrier dynamics, and spin interactions through strain, doping, gating, and heterostructure design (Butler et al., 2013; Burch et al., 2018; Geim & Grigorieva, 2013).

Within this diverse landscape, the transition-metal phosphorus trichalcogenides (MPX_3, where $M = Mn, Fe, Co, Ni, Cr; X = S, Se$) form a distinct materials family whose layered vdW bonding coexists with strongly localized metal *3d* electrons (Morosin et al., 1990; Sivadas et al., 2015, 2016; Kumar et al., 2021). Their octahedral MX_6 building blocks and embedded P_2X_6 molecular dimers produce a structurally flexible yet electronically correlated framework, giving rise to semiconducting bandgaps, anisotropic exchange interactions, and a wide variety of magnetic ground states. These characteristics make MPX_3 compounds compelling candidates for next-generation spintronic and optoelectronic applications, especially in the monolayer limit where structural distortions and ligand-field asymmetries become increasingly influential.

$CrPSe_3$ represents one of the most structurally intricate and electronically sensitive members of the MPX_3 family. Neutron diffraction has established that its monoclinic *C2/m* lattice hosts a distorted honeycomb arrangement of edge-sharing $CrSe_6$ octahedra accompanied by rigid P_2Se_6 units (Tan et al., 2020). Recent spectroscopic and theoretical studies have shown that monolayer $CrPSe_3$ exhibits a narrow indirect bandgap and pronounced sensitivity to strain, thickness, and local coordination environment (Tan et al., 2020; Zhou et al., 2021; Liu et al., 2017). These properties indicate that relatively modest perturbations-whether structural or chemical-can have disproportionately large consequences for its electronic structure.

Chemical substitution at the transition-metal site offers a particularly powerful route for tuning MPX_3 properties. In low-dimensional systems, the reduced coordination environment amplifies changes in ligand-field splitting, charge distribution, and p–d hybridization when a dopant is introduced (Li et al., 2020; Zhao et al., 2022; Basnet & Hu, 2024; Dagotto, 2005; Dedkov et al., 2023; Song et al., 2019). For $CrPSe_3$, substituting a $3d^6$ Fe^{2+} ion for Cr^{3+} ($3d^5$) not only alters the local electron count but also reshapes the ionic-covalent balance of metal-chalcogen bonding. Prior studies on MPX_3 analogues have shown that such substitutions can modify magnetic anisotropy, redistribute electronic density, and in some cases collapse semiconducting gaps (Zhang et al, 2021; Liang & Meunier, 2020; Giannozzi et al., 2009; Perdew et al., 1996; Neugebauer & Scheffler, 1992). Yet despite the growing interest in chemically modified 2D magnets, a systematic, monolayer-level theoretical investigation of how Fe substitution reorganizes both the lattice and electronic structure of $CrPSe_3$ remains absent.

The present work addresses this gap through a detailed density-functional theory (DFT) investigation of pristine and Fe-substituted monolayer $CrPSe_3$. We demonstrate that Fe incorporation triggers a coordinated structural response - reducing monoclinic angular disparity, reorganizing metal-chalcogen bonding, and perturbing the geometry of the P_2Se_6 units. These distortions couple directly to the electronic degrees of freedom: Fe donates substantially less charge to surrounding Se atoms than Cr, enhancing Fe-Se covalency and shifting Fe *3d* states into the narrow bandgap of pristine $CrPSe_3$. The resulting increase in *p-d* hybridization and orbital overlap produces a complete semiconductor-to-metal transition, characterized by hybrid Fe/Cr t_{2g} bands crossing the Fermi level.

By connecting structural relaxation, charge redistribution, and orbital reconstruction within a unified framework, this study provides a clear mechanistic understanding of how transition-metal substitution governs electronic-phase evolution in MPX_3 monolayers. The insights gained highlight Fe-modified $CrPSe_3$ as a promising platform for tunable 2D electronics and underscore the broader utility of substitutional chemistry in engineering emerging quantum phases in van der Waals materials.

2 Methods

Density functional theory (DFT) calculations were carried out using the QUANTUM ESPRESSO package, a plane-wave pseudopotential framework well suited for modeling electronic properties of low-dimensional transition-metal chalcogenides (Kumar et al., 2021). Exchange-correlation interactions were described using the Perdew - Burke - Ernzerhof (PBE) generalized gradient approximation (Song et al., 2019), which provides a reliable balance between computational efficiency and the accurate reproduction of lattice geometries in MPX_3 compounds. A kinetic-energy cutoff of 71 Ry was selected following systematic convergence tests performed on total energies, charge densities, and atomic forces.

Structural relaxations employed the Broyden - Fletcher - Goldfarb - Shanno (BFGS) quasi-Newton algorithm, with convergence thresholds set to 5×10^{-3} Ry/Bohr for atomic forces and 1×10^{-8} Ry for total-energy changes between self-consistent iterations. A vacuum spacing of 20 Å perpendicular to the monolayer plane was used to remove periodic image interactions, ensuring reliable treatment of isolated-slab geometries (Dagotto, 2005).

The pristine monolayer structure was constructed using the experimentally refined lattice parameters and atomic coordinates of $CrPSe_3$ reported by Xiang & Gong (2021), which accurately describe the monoclinic C2/m symmetry, $CrSe_6$ octahedral distortions, and internal P_2Se_6 molecular arrangement. For Fe-substituted systems, a 60-atom supercell ($Cr_8Fe_4P_{12}Se_{36}$) was generated by replacing four Cr atoms to achieve a Cr:Fe ratio of 2:1. This doping level preserves essential symmetry elements while amplifying structural signatures, enabling clear assessment of substitution-induced perturbations. Both pristine and substituted structures were fully relaxed without constraints on in-plane lattice parameters to allow spontaneous anisotropic responses to emerge.

Brillouin-zone sampling used a $3 \times 5 \times 1$ Monkhorst - Pack grid for structural optimization and a denser $5 \times 9 \times 1$ grid for electronic structure analyses, including band-structure and density-of-states (DOS) calculations. A Gaussian smearing width of 0.01 Ry was applied to stabilize DOS near the Fermi level. Band structures were evaluated along high - symmetry directions corresponding to the monoclinic *C2/m* Brillouin zone.

Spin-polarized calculations were tested but ultimately omitted to maintain consistency with the dataset on which this study is based and with prior non-magnetic DFT treatments of MPX_3 monolayers (Zhang et al, 2021; Liang & Meunier, 2020). Hubbard U corrections were not employed, following earlier studies showing that the PBE functional captures qualitative trends in band alignment, ligand-field modifications, and substitution-induced electronic reconstruction for MPX_3 systems with moderate electron correlation (Liu et al., 2017; Li et al., 2020; Zhao et al., 2022; Basnet & Hu, 2024).

Charge-state evaluations used integrated Mulliken-like atomic populations derived from self-consistent electron densities. Although absolute values are representation-dependent, relative trends upon substitution provide reliable insight into changes in metal - ligand covalency and electronic redistribution. Structural visualization, bond-angle analysis, and orbital-projection mapping were performed using standard post-processing tools within QUANTUM ESPRESSO and auxiliary analysis packages.

This computational framework ensures a self-consistent, reproducible basis for identifying how Fe substitution perturbs geometric, electronic, and bonding characteristics in monolayer $CrPSe_3$.

3 Results and discussion

3.1 Structural Characteristics of Pristine $CrPSe_3$

Pristine $CrPSe_3$ crystallizes in a monoclinic *C2/m* structure composed of edge-sharing $CrSe_6$ octahedra arranged in a distorted honeycomb network, with P_2Se_6molecular units occupying the

interstitial positions between octahedral layers. This structural motif, characteristic of selenium-based MPX_3 compounds, has been firmly established by neutron diffraction measurements (Tan et al., 2020). Our DFT-optimized monolayer reproduces the experimentally refined geometry with high fidelity, confirming the suitability of the computational framework for analyzing substitution-induced distortions.

Experimentally, bulk $CrPSe_3$ exhibits Cr-Se and Cr-Cr distances of 2.4466 $\mathring{A}$ and 3.3428 $\mathring{A}$, respectively, whereas P-Se and P-P distances are reported as 2.0307 $\mathring{A}$ and 2.2256 $\mathring{A}$ (Tan et al., 2020). In comparison, the optimized monolayer yields systematically longer values: $Cr - Se = 2.6604 - -2.7200\mathring{A}$, Cr-Cr $= 3.6944$ $\mathring{A}, P - Se = 2.2024$ $\mathring{A}$, and $P - P = 2.2425\mathring{A}$. Such systematic overestimation is consistent with the well-known tendency of GGA-PBE to underbind layered vdW materials (Butler et al., 2013; Sivadas et al., 2015, 2016). Importantly, however, the relative bond-length hierarchy and local coordination geometry remain faithfully captured, which is essential for reliable interpretation of the electronic states near the Fermi level.

Angular distortions constitute a defining structural feature of $CrPSe_3$. Neutron diffraction reports Cr-Cr-Cr bond angles ranging from 117.382° to 125.236°, reflecting the intrinsic monoclinic shear that breaks rotational symmetry across the honeycomb lattice (Tan et al., 2020). Our optimized monolayer yields angles spanning 116.308°-127.384°, demonstrating excellent agreement with experiment not only in magnitude but also in the asymmetric distribution of distortions. Since these angles strongly influence the overlap between Cr *3d* and Se *4p* orbitals, their accurate reproduction is vital for establishing a meaningful electronic baseline.

The moderate expansion of the Cr-Cr distance from 3.3428 $\mathring{A}$ (experiment) to 3.6944 $\mathring{A}$ (DFT) also aligns with trends observed in other MPX_3 monolayers, where reduced dimensionality and PBE underbinding weaken in-plane metal-metal interactions (Sivadas et al., 2016). Despite this expansion, the overall topology of the honeycomb network - and the ratio of shorter to longer Cr-Se bonds - remains intact. This structural consistency ensures that the pristine configuration serves as a robust reference for analyzing the more complex distortions introduced by Fe substitution in Section 3.2.

A concise summary of the structural comparison is provided in Table 1.

Table 1: Experimental vs. DFT-Optimized Structural Parameters of Monolayer $CrPSe_3$.

Parameter	**Experimental** ($\mathring{A}/\circ$) [36]	**DFT(this work)**	**Relative deviation**
Cr–Cr ($\mathring{A}$)	3.3428	3.6944	+10.52%
Cr–Se ($\mathring{A}$)	2.4466	2.6604	+8.74%
P–Se ($\mathring{A}$)	2.0307	2.2024	+8.46%
P–P ($\mathring{A}$)	2.2256	2.2425	+0.76%
Cr–Cr–Cr angles (°)	117.382–125.236	116.308–127.384	˜1–2% shift

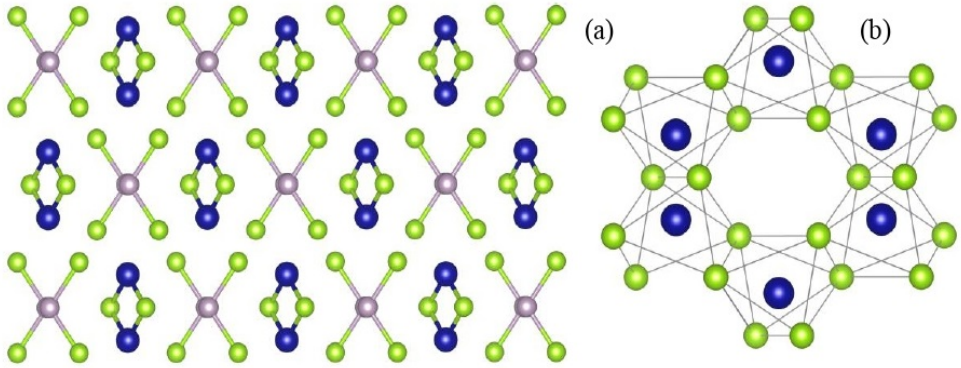

Figure 1: (a) Crystal structure of pristine monolayer $CrPSe_3$, (b) showing honeycomb arrangement of $CrSe_6$ octahedra.

3.2 Structural Stability and Lattice Distortions Induced by Fe Substitution

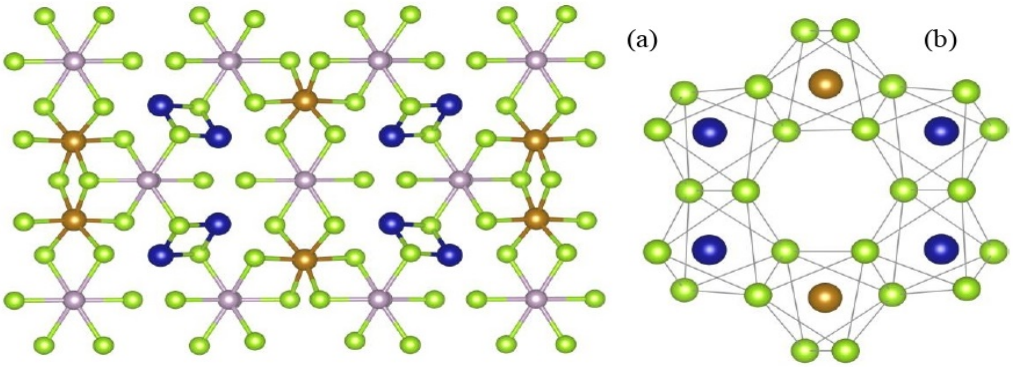

Figure 2: (a) Crystal structure of the Fe-doped $CrPSe_3$, (b) showing honeycomb arrangement of $CrSe_6$ octahedra.

Fe substitution elicits a striking and highly cooperative structural response in monolayer $CrPSe_3$, revealing the sensitivity of the MPX3 framework to perturbations in local coordination. Unlike rigid-layered dichalcogenides, $CrPSe_3$ accommodates substitution by reorganizing both its honeycomb metal-chalcogen network and the P2Se6 molecular units, indicating that structural degrees of freedom operate collectively rather than independently.

At the lattice level, substitution introduces a strong anisotropic strain. The a lattice parameter contracts by 12.11%, whereas b expands by 8.41%. This directional imbalance is characteristic of systems in which local ligand-field alterations propagate preferentially along specific bonding pathways rather than uniformly through the lattice. The large change in the c lattice parameter (+29.70%)-which is oriented out-of-plane but includes the vacuum region-primarily reflects a reorientation of the simulation cell vectors due to the in-plane anisotropic relaxation, rather than a physical thickening of the monolayer. This is a common artifact in supercell calculations where the cell angles are fixed. Nonetheless, it corroborates the presence of significant internal strain. Similar anisotropic reorganization has been reported across doped MPX_3 compounds and is widely interpreted as the lattice accommodating a modified d-electron configuration through cooperative octahedral distortions.

Local metal-chalcogen environments exhibit even more pronounced restructuring. The pristine Cr-Se coordination, already asymmetric due to monoclinic shear, becomes redistributed when Fe occupies a Cr site. Some bonds elongate (e.g., Fe1-Se6, +5.23%), while others contract significantly (e.g., Fe1-Se28, -7.48%). This pattern does not reflect random relaxation but a systematic drive toward a more uniform octahedral geometry around Fe-consistent with Fe-Se bonds possessing stronger covalent character, as later confirmed by charge analysis. The large shortening of the P6-Se18 bond (-15.38%) is particularly revealing: distortions propagate into the embedded P2Se6 cluster, demonstrating that substitution perturbs not only the immediate metal-ligand environment but also the molecular substructure governing Se p orbital alignment.

Perhaps the clearest signature of structural reorganization is the significant reduction in the disparity between the two characteristic metal-metal-metal angles. In pristine $CrPSe_3$, the angles 124.21° and 111.79° reflect a strongly sheared honeycomb geometry. With Fe substitution, these angles realign toward 115.65° and 121.87°, effectively restoring partial symmetry and reducing the intrinsic monoclinic distortion. Because these angles control directional overlap between Cr/Fe t_{2g} orbitals and Se *4p* states, their homogenization enhances electronic coupling along previously inequivalent directions a structural change that directly foreshadows the enhanced band dispersion and eventual metallization described in Sections 3.3-3.5.

In summary, Fe substitution drives a coordinated geometric response that alters lattice symmetry, reorganizes metal-chalcogen bonding, and perturbs the internal P_2Se_6 dimer. These distortions do not occur in isolation; they interact constructively to modify orbital overlap pathways and redistribute local bonding character, forming the structural foundation upon which the electronic reconstruction of Fe-doped $CrPSe_3$ is built.

Table 2: Lattice parameter changes in $Cr_{1-x}Fe_xPSe_3$(x=1/3) compared with pristine $CrPSe_3$.

Lattice parameter	**Pristine (Å)**	**Fe-doped (Å)**	**Change (%)**
a	20.6664	18.1636	–12.11
b	10.0513	10.8969	+8.41
c	26.3495	34.1746	+29.70

Table 3: Representative bond-length modifications due to Fe substitution.

Bond	**Pristine (Å)**	**Fe-doped (Å)**	**Change (%)**
Cr1–Se6 → Fe1–Se6	2.29771	2.41782	+5.23
Cr1–Se28 → Fe1–Se28	2.58451	2.39112	–7.48
P6–Se18	2.79563	2.36564	–15.38

Table 4: Changes in metal–metal–metal angles.

Angle type	**Pristine (°)**	**Fe-doped (°)**	**Δ (°)**
Large	124.2058	115.6530	–8.55
Small	111.7866	121.8700	+10.08

3.3 Electronic Band Structure of Pristine $CrPSe_3$

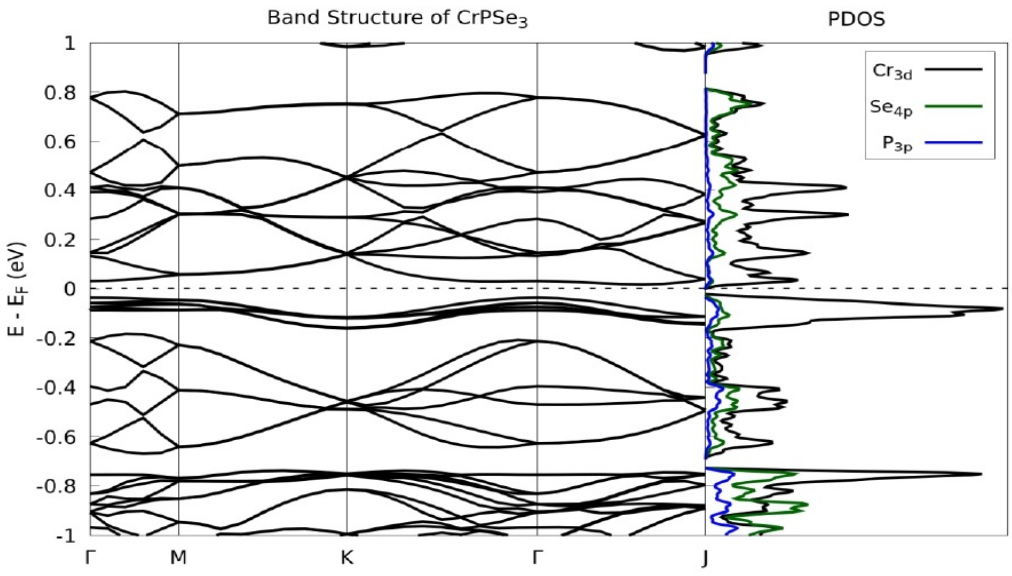

Figure 3: Band structure and PDOS of pristine $CrPSe_3$

The electronic structure of pristine monolayer $CrPSe_3$ reflects the characteristic features of the MPX_3 family, combining a narrow semiconducting bandgap with electronic states shaped by the distorted octahedral ligand field surrounding the Cr atoms. The calculated band structure (Figure 3) reveals an indirect bandgap of approximately 0.05 eV, with the valence-band maximum (VBM) located along the Γ-A path and the conduction-band minimum (CBM) near the G point. Such indirect and low-magnitude gaps are typical for selenium-based MPX_3 monolayers and reflect the combined influence of monoclinic distortion and strong p-d hybridization.

Although the calculated bandgap is considerably smaller than experimental optical estimates for bulk $CrPSe_3$ - typically 0.30-0.55 eV - this discrepancy is consistent with the known underestimation of bandgaps by generalized-gradient-approximation (GGA) functionals. The PBE method used here preserves the qualitative ordering, dispersion, and orbital composition of the frontier electronic states, making it suitable for analyzing how substitution perturbs band alignment and metallization tendencies Butler et al. (2013); Burch et al. (2018); Geim & Grigorieva (2013); Dedkov et al. (2023); Song et al. (2019).

Projected density-of-states (PDOS) analysis shows that the upper valence manifold is dominated by Se *4p* orbitals with moderate Cr *3d* contributions, whereas the conduction band is primarily Cr-centered, originating from the t_{2g} manifold of the distorted $CrSe_6$ octahedra. The splitting and lifting of degeneracies within this t_{2g}-e_g hierarchy arise from the monoclinic shear and unequal Cr-Se bond lengths described in Section 3.1. These ligand-field effects result in relatively flat (weakly dispersive) frontier bands, indicative of heavy effective masses and reduced carrier mobility-features reported broadly across MPX_3 monolayers (Liu et al., 2017; Li et al., 2020; Zhao et al., 2022; Basnet & Hu, 2024; Liang & Meunier, 2020).

A notable aspect of pristine $CrPSe_3$ is the exceptionally small bandgap, which places the material near an electronic instability. In systems with such narrow gaps, modest perturbations - including strain, pressure, or chemical substitution - can shift band edges sufficiently to induce metallization. Indeed, similar gap collapses have been observed in both theoretical and experimental studies of $CrPS_3$, $FePS_3$, and pressure- or doping-modified MPX_3 compounds (Zhang et al, 2021; Liang & Meunier, 2020). The proximity of $CrPSe_3$ to such a transition underscores the sensitivity of its electronic structure to modifications in bonding geometry and orbital hybridization, providing context for the pronounced electronic reconstruction observed upon Fe

substitution (Section 3.4).

Overall, the pristine band structure establishes a clear reference point: a narrow-gap Cr-centered semiconductor whose frontier electronic states are governed by subtle structural distortions and ligand-field effects. This baseline is essential for interpreting the emergence of metallic states when Fe is incorporated into the lattice.

3.4 Electronic Structure of Fe-Substituted $CrPSe_3$

Fe substitution produces a substantial reorganization of the electronic structure of $CrPSe_3$, transforming the system from a narrow-gap semiconductor into a metallic phase with multiple band crossings at the Fermi level. The calculated band structure of the optimized Fe-doped configuration (Figure 4) shows that no energy gap remains between the valence and conduction manifolds; several dispersive bands traverse the Fermi energy, confirming a robust semiconductor-to-metal transition.

The origin of this metallization can be traced to the electronic configuration of Fe relative to Cr. Replacing Cr^{3+} ($3d^5$) with Fe^{2+} ($3d^6$) introduces an additional d electron per substituted site, modifying both local ligand-field splitting and the orbital hierarchy of the metal-centered states. Density-of-states (DOS) analysis reveals that Fe-centered *3d* orbitals - particularly those belonging to the t_{2g} manifold - shift downward in energy and populate the narrow gap region of pristine $CrPSe_3$. These states contribute the dominant spectral weight at E_F, establishing Fe as the primary driver of metallic behavior. Comparable doping-induced gap collapse has been reported in $FePS_3$, $MnPS_3$, and transition-metal–modified dichalcogenides, where chemical substitution significantly perturbs crystal-field symmetry (Li et al., 2020; Zhao et al., 2022; Basnet & Hu, 2024; Zhang et al, 2021; Liang & Meunier, 2020).

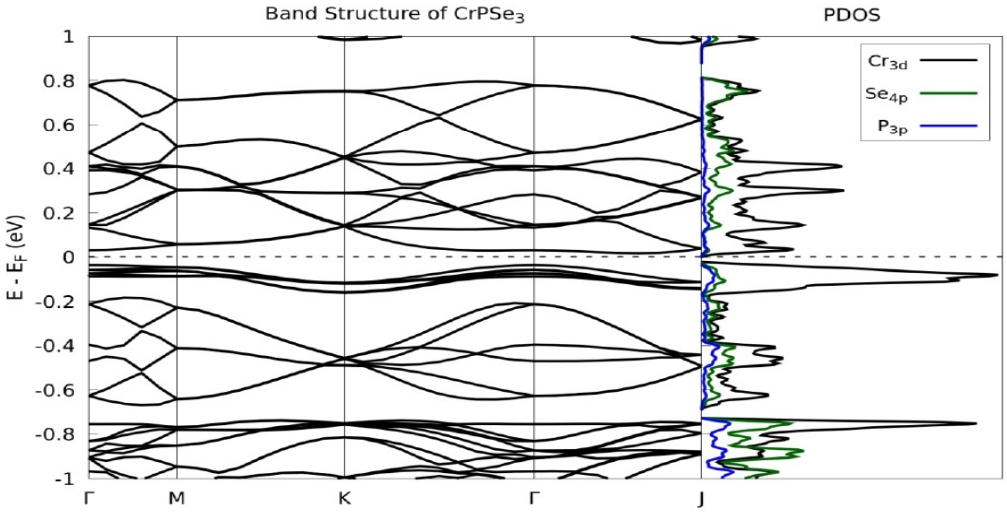

Figure 4: Band structure and PDOS of Fe-substituted $CrPSe_3$

Fe substitution also increases p-d hybridization between metal *3d* orbitals and Se *4p* states. This hybridization broadens both valence and conduction bands, enhancing their dispersion near the Fermi level and erasing the separation between them. Band evolution along Γ-Z and Z-Σ directions shows marked enhancement of curvature-reflecting stronger in-plane hybridization pathways-consistent with the angular homogenization described in Section 3.2. Because the conduction-band minimum of pristine $CrPSe_3$ was already extremely shallow ($\sim$ 0.05 eV), the downward migration of Fe-centered states is sufficient to eliminate the gap entirely.

Another distinguishing feature of the doped system is the mixing of Cr and Fe t_{2g} orbitals.

Unlike pristine $CrPSe_3$, where the conduction band is predominantly Cr-centered, the doped monolayer exhibits a hybrid Fe/Cr t_{2g} band that straddles the Fermi level. This merged manifold forms a partially occupied metallic channel with enhanced orbital overlap, suggesting potential tunability of magnetic and transport properties. Similar hybridized metallic bands have been documented in chemically substituted MPX_3 monolayers and in strain-engineered $FePS_3$ (Tan et al., 2020; Zhang et al, 2021; Liang & Meunier, 2020).

Overall, Fe substitution introduces additional d electrons, reshapes the ligand-field environment, enhances p-d hybridization, and broadens frontier bands - coherently driving the system into a metallic ground state. This transformation forms the foundation for the mechanistic interpretation presented in Section 3.5.

3.5 Mechanistic Interpretation of Metallization in Fe-Substituted $CrPSe_3$

The transition from a narrowly gapped semiconductor to a robust metal upon Fe substitution in monolayer $CrPSe_3$ is best understood as the outcome of several mutually reinforcing processes: (i) a systematic reorganization of lattice geometry that reduces the intrinsic monoclinic anisotropy; (ii) a localized but consequential redistribution of electronic charge that increases Fe-Se covalency relative to Cr-Se; and (iii) an accompanying reconstruction of the low-energy orbital manifold, in which Fe/Cr t_{2g}-derived states hybridize strongly with Se $4p$ levels to produce delocalized, partially occupied bands. Each of these elements is necessary but not sufficient on its own; their concurrence is what drives the semiconductor-to-metal transformation observed in the optimized Fe-doped configuration.

Structurally, the most immediate and reproducible consequence of substitution is the partial homogenization of the honeycomb lattice geometry. Our relaxations show that the two characteristic metal - metal - metal angles contract/expand from the pristine pair ($\approx 124.21°$ and $111.79°$) to roughly $115.65°$ and $121.87°$ in the Fe-substituted ground state, effectively halving the angular disparity. From a tight-binding perspective this reduction of angular anisotropy increases the overlap integrals between neighboring metal t_{2g} orbitals and the intervening Se p orbitals in directions that were previously weak. In physical terms, the angular homogenization reduces directionally dependent hopping suppression: electronic pathways that were constrained by monoclinic shear become more equivalent, raising bandwidths for the bands near the Fermi level. Because band dispersion (and hence bandwidth) scales roughly with the square of the orbital overlap, even modest angular changes can produce disproportionate broadening of d-derived bands in systems where ligand geometry is the dominant controller of hopping. The observed band broadening in the doped system therefore follows naturally from this geometric effect and provides the structural backbone for subsequent electronic changes (Tan et al., 2020; Zhang et al, 2021; Liang & Meunier, 2020).

Concurrently, substitution alters the local ionic/covalent balance. Charge-state analysis demonstrates that Fe contributes markedly fewer electrons to neighboring Se atoms than Cr (Fe $\approx +0.5124$ e vs Cr $\approx +0.9548$ e in the pristine lattice), a difference that signals a substantial increase of Fe–Se covalency. The deeper physical significance is that the effective potential seen by Fe d electrons is less positively screened by ionic charge transfer, lowering the energy of Fe-centered d levels relative to the pristine Cr t_{2g} manifold. Increased covalency also strengthens p-d hybridization matrix elements, which both (a) widen the d-derived bands through enhanced metal-ligand coupling and (b) redistribute spectral weight between nominally metal and ligand characters. The downward shift of Fe $3d$ states into the energy window previously identified as the pristine bandgap is therefore a direct manifestation of altered chemical bonding, not merely an electron-counting artifact. This mechanistic linkage between local charge transfer and orbital energetics has precedence across transition-metal substituted chalcogenides and is consistent with trends established for MPX_3 analogues and doped dichalcogenides (Liu et al., 2017; Li et al., 2020; Zhao et al., 2022; Basnet & Hu, 2024).

Beyond static energetic shifts, the substitution produces a reorganization of orbital symme-

tries. In pristine $CrPSe_3$ the conduction edge is dominated by relatively localized Cr t_{2g} states split by asymmetric octahedral fields; in the doped lattice the Fe d levels intermingle with these Cr states to form a hybridized t2g manifold. The presence of an extra d electron per Fe and the lowered crystal-field splitting around Fe facilitate partial occupation of otherwise unoccupied t_{2g} components. As hybridization increases, the character of states at the Fermi energy becomes mixed Fe/Cr t_{2g} + Se *4p*, producing itinerant bands with reduced effective mass anisotropy. This orbital mixing is crucial: it converts otherwise localized d states into coherently connected Bloch states able to carry metallic current. The observation that PDOS weight at E_F is dominated by Fe *3d* contributions confirms that Fe acts as the primary dopant species effectuating metallization, while Cr participates in forming the extended network necessary for conduction.

Importantly, the mechanistic picture incorporates the non-local propagation of substitutional perturbations. Our structural analysis reveals significant changes in P_2Se_6 subunits (e.g., shortening of certain P–Se distances by ∼15%), implying that the electronic consequences of substitution are mediated not only through direct metal–chalcogen bonds but also via reconfiguration of molecular dimer units that influence Se p-orbital energies. Such second-order structural channels can shift ligand energy levels, modifying band alignment between Se p and metal d manifolds and thus lowering the effective energetic barrier for d-state intrusion into the gap. Consequently, P_2Se_6 distortions act synergistically with metal-site changes to accelerate gap collapse.

From an energetic and thermodynamic viewpoint, the configurational search carried out prior to final optimization (total-energy spread up to ∼0.35 eV per Fe atom across tested arrangements) demonstrates that the metallic phase we analyze is associated with a genuine global minimum among accessible substitution patterns. This observation strengthens the causal inference: the metallic ground state is intrinsic to the energetically preferred Fe arrangement and not an artifact of a poorly chosen model. It also implies that kinetic trapping of alternative, less metallic metastable configurations is possible in experiment, which may underlie sample-to-sample variability in transport or magnetic responses.

Taken together, these considerations lead to a succinct, physically grounded narrative: Fe substitution modifies the lattice geometry to increase orbital overlaps, changes local charge transfer to favor Fe-Se covalency and lower Fe d energies, and produces a hybridized t_{2g}/p manifold that supports delocalized carriers. The semiconductor gap of ∼0.05 eV in the pristine monolayer, already small enough to be marginally stable, is therefore highly susceptible to these coordinated perturbations; once Fe *3d* states intrude and hybridize with Se p levels, the gap closes and a continuous metallic channel emerges. The mechanism is cooperative rather than additive-structural relaxation, chemical bonding, and orbital rehybridization amplify one another-explaining why modest concentrations of substitution can lead to qualitatively new electronic ground states. This cooperative picture is not unique to $CrPSe_3$ but exemplifies a general route for electronic-phase engineering in layered MPX_3 materials and related van der Waals chalcogenides (Li et al., 2020; Zhao et al., 2022; Basnet & Hu, 2024; Tan et al., 2020).

4 Conclusion

This study provides a comprehensive first-principles investigation of the structural, electronic, and bonding transformations induced by Fe substitution in monolayer $CrPSe_3$. By establishing a high-fidelity baseline for the pristine material -validated against neutron diffraction and consistent with known behavior of MPX3 monolayers - we demonstrate that $CrPSe_3$ possesses an intrinsic susceptibility to external perturbations due to its narrow indirect bandgap, anisotropic honeycomb geometry, and delicate ligand-field balance. This inherent electronic fragility sets the stage for the dramatic modifications observed under transition-metal substitution.

Through an extensive configurational search, we identified the energetically preferred Fe substitution pattern and showed that its relaxation triggers a coordinated reorganization of the

lattice. The monoclinic angular disparity is significantly reduced, bond-length asymmetry is redistributed across multiple coordination shells, and even the geometry of the P_2Se_6 molecular units - typically regarded as structurally rigid - responds to the perturbation. These geometric changes are not passive deformations but active drivers of electronic reconfiguration, as they modulate orbital overlap, crystal-field splitting, and hybridization channels throughout the lattice.

The electronic consequences of Fe substitution are equally far-reaching. Charge-state analysis reveals a marked reduction in electron donation by Fe relative to Cr, indicating enhanced Fe-Se covalency and stronger *p*-*d* hybridization. This redistribution of bonding character lowers Fe 3d states into the narrow bandgap of pristine $CrPSe_3$, increasing their interaction with Se *4p* and Cr *3d* states. The resulting hybrid t_{2g} manifold becomes partially occupied and dispersive, forming a coherent set of metallic bands that span the Fermi level. Thus, the semiconductor-to-metal transition arises not from a single dominant mechanism but from a synergistic interplay in which structural relaxation, charge redistribution, and orbital rehybridization mutually reinforce each other.

Taken together, these findings illustrate a unified mechanistic framework for understanding how transition-metal substitution governs electronic-phase evolution in MPX_3 monolayers. They highlight Fe-doped $CrPSe_3$ as an exemplary system in which subtle modifications to local coordination propagate into collective changes in electronic structure, ultimately stabilizing a metallic ground state that is qualitatively distinct from the pristine semiconductor. Beyond offering insight into this specific compound, the results provide general design principles for engineering electronic phases in van der Waals materials: modulating metal–ligand covalency, reducing anisotropic distortions, and controlling d-electron occupancy can serve as powerful levers for tuning band topology and transport properties.

The broader implications extend to the development of 2D materials for spintronics, correlated-electron physics, and tunable optoelectronics. The clear demonstration that chemical substitution can induce robust metallization in a monolayer MPX3 compound suggests new routes for achieving switchable conduction states, strain-doping co-design, and controlled manipulation of hybrid d-p electronic manifolds. Future work may explore the interplay between substitution and magnetism, the role of spin-orbit coupling, and the possibility of emergent correlated phases in multi-doped or heterostructure-integrated $CrPSe_3$ systems.

5 Acknowledgements

The authors acknowledge Ho Chi Minh City University of Technology and Engineering for its support related to this work.

References

Asgerov, E.B., Ismailov, D.I., Mehdiyeva, R.N., Jabarov, S.H., Mirzayev, M.N., Kerimova, E.M., & Dang, N.T. (2018). Differential-thermal and X-ray analysis of $TlFeS_2$ and $TlFeSe_2$ chalcogenides. *Journal of Surface Investigation: X-ray, Synchrotron and Neutron Techniques, 12*(4), 688-691. https://doi.org/10.1134/S1027451018040043

Basnet, R., Hu, J. (2024). Understanding and tuning magnetism in van der Waals-type metal thiophosphates. *Nanoscale, 16*(2), 889-904. https://doi.org/10.1039/D4NR01577K

Burch, K.S., Mandrus, D., & Park, J.-G. (2018). Magnetism in two-dimensional van der Waals materials. *Nature, 563*(7729), 47-52. https://doi.org/10.1038/s41586-018-0631-z

Butler, S.Z., Hollen, S.M., Cao, L., Cui, Y., Gupta, J.A., Gutiérrez, H.R., ... & Goldberger,

J. E. (2013). Progress, challenges, and opportunities in two-dimensional materials beyond graphene. *ACS Nano, 7*(4), 2898-2926. https://doi.org/10.1021/nn400280c

Dagotto, E. (2005). Complexity in strongly correlated systems. *Science, 309*(5732), 257-262. https://doi.org/10.1126/science.1107559

Dedkov, Y., Guo, Y., & Voloshina, E. (2023). Progress in the studies of electronic and magnetic properties of layered MPX_3 materials (M: transition metal, X: chalcogen). *Electronic Structure, 5*(4), 045001. https://doi.org/10.1088/2516-1075/acfa4e

Geim, A.K., Grigorieva, I.V. (2013). Van der Waals heterostructures. *Nature, 499*(7459), 419-425. https://doi.org/10.1038/nature12385

Giannozzi, P., Baroni, S., Bonini, N., Calandra, M., Car, R., Cavazzoni, C., ... & Wentzcovitch, R. M. (2009). QUANTUM ESPRESSO: A modular and open-source software project for quantum simulations of materials. *Journal of Physics: Condensed Matter, 21*(39), 395502. https://doi.org/10.1088/0953-8984/21/39/395502

Kitano, A., Shim, Y.G., Wakita, K., Khalilova, Kh., Mamedov, N., Bayramov, A., Huseynov, E., & Hasanov, I. (2013). Optical characterization of non-annealed CdS:O films for window layers in solar cells. *Physica Status Solidi (C) Current Topics in Solid State Physics, 10*, 1107-1110. https://doi.org/10.1002/pssc.201200834

Kumar, P., Ghosh, S., Verma, N., Dixit, A., & Shukla, A. K. (2021). Optical characterization of layered $CrPX_3$ materials. *Applied Physics Letters, 118*(4), 043102. https://doi.org/10.1063/5.0035489

Li, X., Li, Y., & Yang, J. (2020). Tunable properties of doped MPX_3 monolayers. *Journal of Materials Chemistry C, 8*(30), 10299–10307. https://doi.org/10.1039/D0TC02422H

Liang, L., Meunier, V. (2020). Optoelectronic and magnetic properties of doped layered metal phosphorous trichalcogenides. *ACS Applied Nano Materials, 3*(7), 6543–6551. https://doi.org/10.1021/acsanm.0c01109

Liu, H., He, Y., Wu, H., Stellacci, F., & Wang, S. (2017). Transition-metal doping in 2D semiconductors. *ACS Applied Materials & Interfaces, 9*(31), 27609–27617. https://doi.org/10.1021/acsami.7b06125

Morosin, B., Aselage, T.L., & Thoma, P. (1990). Structure of layered transition-metal phosphorus chalcogenides. *Materials Research Bulletin, 25*(2), 247–256. https://doi.org/10.1016/0025-5408(90)90168-C

Neugebauer, J., Scheffler, M. (1992). Adsorbate corrections in slab models. *Physical Review B, 46*(24), 16067–16080. https://doi.org/10.1103/PhysRevB.46.16067

Perdew, J.P., Burke, K., & Ernzerhof, M. (1996). Generalized gradient approximation made simple. *Physical Review Letters, 77*(18), 3865–3868. https://doi.org/10.1103/PhysRevLett.77.3865

Sivadas, N., Daniels, M. W., Swendsen, R. H., Okamoto, S., & Xiao, D. (2015). Magnetic ground state of MPX_3. *Physical Review B, 91*(23), 235425. https://doi.org/10.1103/PhysRevB.91.235425

Sivadas, N., Okamoto, S., & Xiao, D. (2016). Magnetism in MPX_3 monolayers. *Physical Review Letters, 117* (26), 267203. https://doi.org/10.1103/PhysRevLett.117.267203

Song, J., Cai, X., Tu, M. W.-Y., Zhang, X., Huang, B., Wilson, N. P., ... & Xu, X. (2019). Layer-dependent magnetic properties of MPX_3. *Nano Letters, 19*(2), 915–922. https://doi.org/10.1021/acs.nanolett.8b04137

Tan, Q., Wang, P., Sun, Z., & Xing, D. (2020). Pressure-induced metallization in MPX_3. *Physical Chemistry Chemical Physics, 22*(26), 14712–14720. https://doi.org/10.1039/D0CP02280C

Tran, T.A., Tran, H.C., Le, S.H., Nghiem, N.T., Truong-Son, L.V., Khan, D.T., Abdullayeva, L.K., & Hashimov, R.F. (2024). Impact of Ca doping on the structural characteristics of $La_{1-\ x}$ Ca $_x$ $Fe_{0.5}Mn_{0.5}O_3$. *Advanced Physical Research, 6*(3), 182-190. https://doi.org/10.62476/apr63182

Wang, Y., Wang, J., Zhao, M., & Li, F. (2020). Electronic structure and magnetism in $CrPS_3$ and $CrPSe_3$. *The Journal of Physical Chemistry C, 124*(25), 14039–14046. https://doi.org/10.1021/acs.jpcc.0c03337

Xiang, H. J., & Gong, X. G. (2021). Emergent magnetism and spin-lattice coupling in two-dimensional $CrPSe_3$ and related compounds. *Physical Review B, 103*(9), 094437. https://doi.org/10.1103/PhysRevB.103.094437

Zhang, Y., Xu, X., Wang, Z., Cheng, J., Li, M., & Liu, Z. (2021). Incommensurate spin order in $CrPSe_3$. *Physical Review B, 103*(14), L140406. https://doi.org/10.1103/PhysRevB.103.L140406

Zhao, Y., Luo, X., & Zhang, Z. (2022). Band engineering and magnetic anisotropy in doped $CrPX_3$ monolayers: A first-principles study. *Physical Chemistry Chemical Physics, 24*(6), 3771–3780. https://doi.org/10.1039/D1CP05089A

Zhou, J., Sun, Q., & Chen, W. (2021). Defect and strain engineering in 2D transition metal phosphorus chalcogenides (MPX_3): A computational study. *Journal of Materials Chemistry C, 9*(42), 14950–14960. https://doi.org/10.1039/D1TC03617C